Effect of thickness on the photoluminescence of silicon quantum dots embedded in silicon nitride films

A. Rodriguez-Gómez, A. García-Valenzuela, E. Haro-Poniatowski, and J. C. Alonso-Huitrón

Citation: Journal of Applied Physics **113**, 233102 (2013); doi: 10.1063/1.4811361
View online: http://dx.doi.org/10.1063/1.4811361
View Table of Contents: http://scitation.aip.org/content/aip/journal/jap/113/23?ver=pdfcov
Published by the AIP Publishing

Effect of thickness on the photoluminescence of silicon quantum dots embedded in silicon nitride films

A. Rodriguez-Gómez,[1] A. García-Valenzuela,[2] E. Haro-Poniatowski,[3] and J. C. Alonso-Huitrón[1,a)]

[1]*Instituto de Investigaciones en Materiales, Universidad Nacional Autónoma de México, Apartado Postal 70-360, Coyoacán 04510, Distrito Federal, Mexico*

[2]*Cenro de Ciencias Aplicadas y Desarrollo Tecnológico, Universidad Nacional Autónoma de México, Apartado Postal 70-186, Coyoacán 04510, Distrito Federal, Mexico*

[3]*Departamento de Física, Universidad Autónoma Metropolitana, Iztapalapa, Av. San Rafael Atlixco No. 186, Col Vicentina A.P. 09340, Distrito Federal, Mexico*

(Received 3 April 2013; accepted 3 June 2013; published online 18 June 2013)

In this work, the effect of film thickness on the photoluminescence (PL) spectra of Si quantum dots embedded in silicon nitride films is investigated experimentally and theoretically. The films were deposited by remote plasma enhanced chemical vapor deposition using the same $SiH_2Cl_2/H_2/Ar/NH_3$ mixture and deposition conditions, in order to obtain films with similar composition and approximately equal average size (~3.1 nm) of Si quantum dots. Only the deposition times were varied to prepare five samples with different thicknesses ranging from ~30 nm to 4500 nm. Chemical characterization by Fourier Transform Infrared Spectroscopy and X-ray Photoelectron Spectroscopy were carried out in order to check that the composition in all films was the same. The structure, average size, and size distribution of the Si quantum dots were deduced from High-Resolution Transmission Electron Microscopy. The thickness of the films was determined by ellipsometry and interferometry of UV-Vis transmission spectra. It was found experimentally that the increase of the thickness above a few hundreds of nanometers produces significant distortions of the PL spectra of the films, such as peak shifts and the appearance of shoulders and multiple peaks suggesting interference effects. Comparing the experimental results with theoretical simulations, it is shown that these distortions are mainly due to interference effects and not to intrinsic changes in the films. The approximation used to simulate the PL spectra as a function of film thickness allows improving the fitting between simulated and experimental spectra by changing some optical parameters and can be helpful to further investigate the intrinsic optical properties of the films. © *2013 AIP Publishing LLC*. [http://dx.doi.org/10.1063/1.4811361]

I. INTRODUCTION

The preparation and investigation of luminescent silicon nitride (SiN_x) thin films containing silicon quantum dots (Si QDs) and/or excess of silicon ($x < 1.33$) has gained increasing interest during the last years, with the purpose of developing low-cost, reliable, and efficient silicon-based photonic, optoelectronic, and photovoltaic devices.[1–6] Although there is growing consensus that the photoluminescence (PL) of silicon quantum dots embedded in silicon nitride (Si QDs/SiN_x) films is mainly due to quantum confinement effects,[7–15] other alternative models have been proposed. According to these models, the PL has different origins: radiative electron-hole recombination between hydrogen and nitrogen–related chemical bonds at the surface of the Si nanoclusters,[2,12] localized band-tail states of the silicon nitride film,[16–18] and also defect centers or dangling bonds in the silicon nitride matrix.[19–22] A detailed revision of the corresponding literature reveals two important elements that have generated debate on the origin of the PL in these Si-nanostructured films. First, the appearance of shoulders and/or multiple peaks in some of the PL spectra obtained experimentally. Second, the comparison and modeling of these spectra, under the assumption that the PL features depend only on the intrinsic properties of the films and not on extrinsic properties such as their thickness. As an example, some works reporting several peaks in the PL spectra of SiN_x films (with thickness ~350–380 nm) have suggested that it is necessary to make distinction between luminescence peaks that are originated from the Si QDs and those coming from the silicon nitride matrix.[13,21] Other similar works have concluded that the appearance of several or multiple peaks in the PL spectra of SiN_x films (with thickness ~610 nm) is an evidence that the PL is originated from several or multiple dangling bond defects.[19,20] In spite of this, there are other works that have proposed that the multiple peaks in the PL spectra might come from one broad peak of light emitted by the Si QDs modulated by interference of multiple beam reflections in the films, when these have thicknesses of few hundreds nanometers.[18,19,23] In a previous work, it has been also pointed out that Si QDs/SiN_x films thinner than 100 nm (~80 nm) must be chosen in order to avoid interference effects on the PL spectra.[15] In the case of buried layers of Si nanocrystals (Si-nc) implanted in silica and SiO_2 layers, interference effects in the optical absorption and reflectivity

a)Author to whom correspondence should be addressed. Electronic mail: alonso@unam.mx

spectra, as well as distortions in the PL spectra (appearance of shoulders and/ multiple peaks), have been qualitatively demonstrated and investigated as a function of sample thickness.[24,25] For this Si-nc/SiO_2 layer system, simulations of optical modulation effects on the PL spectra have been developed, showing how these PL spectra can be dramatically influenced by optical-geometrical effects, such as layer thickness, refractive index, geometry of the excitation, etc.[26] However, to our knowledge, there are not dedicated studies or simulations of the optical-geometrical effects on the PL spectra of Si QDs embedded in SiN_x films.

In this work, the effect of thickness on the PL spectra of samples of Si-QDs embedded in chlorinated-silicon nitride (SiN_x:Cl) thin films, deposited by remote plasma enhanced chemical vapor deposition (RPECVD) is investigated. We report the experimental PL spectra of films with the same average size of Si QDs (~3.1 nm) and composition of the SiN_x matrix, but with five different thickness that vary from ~30 nm to ~4500 nm. Finally, a theoretical simulation was performed in order to demonstrate that the features of the spectra, particularly, the appearance of multiple peaks is drastically affected by the thickness of the films due to optical interference.

II. EXPERIMENT

The thin films used in this work were prepared using an RPECVD system designed by ourselves and manufactured by the company MV-Systems Inc. (Colorado, USA). The system is schematically shown in Figure 1. It is constituted by a low volume load chamber and a vacuum-deposition chamber (DCH) of 26500 cm^3, at the highest part of the DCH is a quartz tube 10.6 cm in diameter and 20 cm height, surrounded by a water-cooled copper coil, which is responsible for the power transfer from the radio frequency (RF) source to the plasma. The coupled source operates with a frequency of 13.56 MHz and a power range from 0 to 500 watts. The vacuum system of the DCH is a turbomolecular-mechanical vacuum-pump arrangement, which is able to provide a base pressure of 10^{-6} Torr and the pressure is

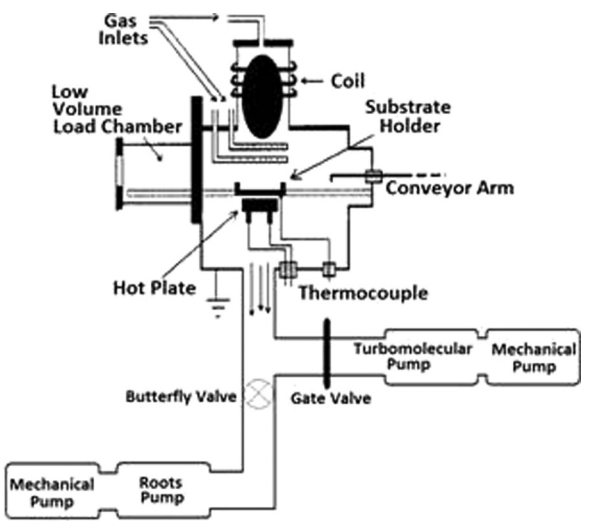

FIG. 1. Schematic diagram of the RPECVD system used to fabricate the samples.

adjustable in the range of 10^{-6}–10^{-2} Torr through a butterfly valve operated by an automatic proportional controller. The substrate holder inside of the DCH is a boron-nitride hot plate controlled by a temperature system that allows a range from room temperature to 700 °C. The flow rates of the gases are controlled automatically by MKS electronic mass-flow meters.

The films were deposited on high resistivity (200 Ω cm) single crystalline silicon wafer n-type (100) (Si-substrate) and quartz substrates. Prior to deposition, Si-substrates were cleaned for 5 min using a "p-etch solution" reported elsewhere,[27] while quartz substrates were cleaned by submerging them in acetone for an ultrasonic bath for 5 min and rinsing with distilled water. For all the samples, we used the same gas mixture of $SiH_2Cl_2/H_2/Ar/NH_3$. The flow rate of these gases was 5, 20, 150, and 200 sccm, respectively, the gases Ar and NH_3 were fed from the top of the deposition chamber where the plasma is formed; meanwhile, gases SiH_2Cl_2 and H_2 were fed from the side and underneath the plasma through the use of a dispersal ring located over the substrate holder. The remaining deposition parameters were also the same for all the deposits and they were as follows: substrate temperature 300 °C, total pressure 300 mTorr, and RF power 300 watts. We set the same deposition conditions in all the deposited films in order to maintain the same average size of Si-QDs; but we used five different deposition times, varying from 1.5 min to 2.7 h, to obtain films with very different thicknesses.

The thickness and refractive index of the films were measured by ellipsometry using a Gaertner L117 Ellipsometer equipped with a He–Ne laser ($\lambda = 632.8$ nm) at an incidence angle of 70°. Chemical bond analysis was determined using a Fourier Transform Infrared Spectrophotometer (FTIR) Nicolet 210 operated in the range of 400–4000 cm^{-1} with a resolution of 2 cm^{-1}. X-ray photoelectron spectroscopy analysis (XPS) of the composition (N/Si ratio and Cl%) was performed by means of a VG Microtech Multilab ESCA 2000 system. PL measurements were carried out by exciting with a Kimmon He-Cd laser beam with a wavelength of 325 nm and a power of 25 mW, and these spectra were recorded with a Fluoromax-Spex spectrofluorometer. The incident angle of the excitation beam was 45° and the detection of the emitted light was in the direction normal to the film surface. The High-Resolution Transmission Electron Microscopy (HRTEM) analysis was performed at the Institute of Physics-UNAM's using a JEOL JEM-2010F FasTEM microscope operating at 200 KV near the Scherzer focus, with a spherical aberration of 0.5 mm, a theoretical point to point resolution of 0.20 nm and equipped with a GATAN digital micrograph system for image acquisition (version 3.7.0). Ultraviolet–visible (UV–vis) transmission measurements were done in the range from 300 to 1100 nm using a double-beam PerkinElmer Lambda 35 UV–vis spectrophotometer.

III. EXPERIMENTAL RESULTS AND ANALYSIS

A. Composition and structure of the films

The values of thickness and refractive index measured by ellipsometry for all the samples are shown in Table I. The

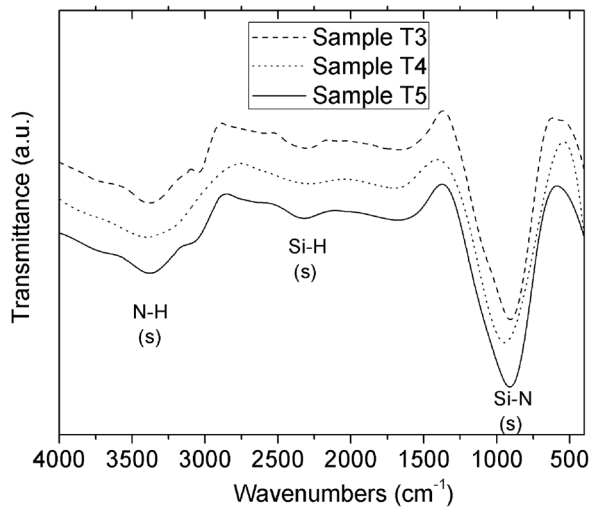

FIG. 2. FTIR transmission spectrum of samples T3, T4, and T5.

N/Si ratios and Cl at. % for the films determined by XPS are also shown in this table. The FTIR spectra of the three thicker films are shown in Fig. 2. The FTIR spectra of the thinnest samples are not worth of showing because they are of very poor quality given their low signal to noise ratio. The three FTIR spectra are characteristic of silicon nitride films, since all of them show an absorption band located at 863 cm^{-1}, which is associated to stretching vibration of Si-N bonds, and a band at 3356 cm^{-1} attributable to stretching vibration of N-H bonds. The 2205 cm^{-1} signal is associated to stretching modes of Si-H bonds indicating some degree of passivation of the silicon nanoclusters with hydrogen. Absorption bands between 500 and 650 cm^{-1} corresponding to Si-Cl bond were not detected. This fact is not an indicative of absence of chlorine in the films; it is rather that those signals must be veiled by the width of Si-N band. Although, the FTIR technique could be insensitive to small changes in the Si excess or composition of the films, the similarity among the three FTIR spectra suggests that the type and amount of bonds is almost the same in all the films, independently of their thickness. On the other hand, as it can be seen from Table I, the refractive index, N/Si ratios, and Cl at. % are very close for all the films. Considering the uncertainty of these measurements, we can infer that the composition and intrinsic structure of the films is practically the same for all the samples, this was expected since they were prepared under the same deposition conditions, and only the deposition time was varied. At this point, it is important to mention that the XPS technique provides information of a very thin sublayer at the top surface of each film. However, the deposition of each complete film can be visualized as the superposition of very thin sublayers, whose number increases during the deposition time. The fact that the composition of the top surface layer does not change with film thickness is indicative that all the films have the same composition.

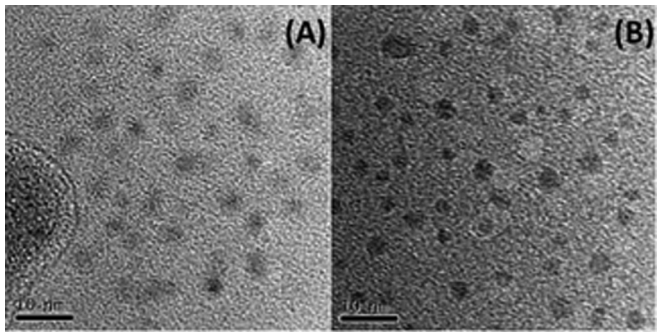

FIG. 3. HRTEM micrograph for (a) sample T1 and (b) sample T5. Both samples have the same Si-nanocluster average size of 3.1 nm.

HRTEM analysis were performed in order to check that the average size, size distribution, and density of silicon nanoparticles embedded in the silicon nitride films were independent of film thickness. Due to the time consuming nature of this characterization, just two samples T1 and T5 were observed, and it was assumed that films with intermediate values of thicknesses had the same structural characteristics.

Figure 3 shows the HRTEM micrographs for (a) sample T1 and (b) sample T5. The low contrast between the silicon nitride matrix and the Si nanoclusters observed in the HRTEM images, precluded the use of any software for counting and making statistics of embedded nanoclusters in our samples; therefore, the calculation of average size and particle density was performed manually counting 76 and 91 micrographs for the samples T1 and T5, respectively. The diameters of 1545 and 1802 particles corresponding to samples T1 and T5 were measured. By doing this statistical analysis, an average size of 3.102 nm for sample T1 and 3.125 nm for sample T5 were obtained. The histogram reported in Figure 4 was generated by grouping Si nanoparticles in the ranges of 1–2 nm, 2–3 nm, 3–4 nm, 5–6 nm, and >6 nm, and calculating the probabilities of their appearance in each of these ranges. For T1, the probabilities of appearance were: 0.0642, 0.4250, 0.3870, 0.1100, and 0.0138, respectively; while for T5, they were: 0.0640, 0.4252, 0.3864, 0.1106, and 0.0138, respectively. The high similarity of the two histograms makes them practically the same and

TABLE I. Main characteristics of the samples.

Sample	Thickness (nm) (ellipsometry)	Refractive index (ellipsometry)	N/Si ratio (XPS)	%Cl (XPS)	Wavelengths of PL peaks (nm) (from PL spectra)
T1	31	1.82	1.07	5.3	469
T2	95	1.83	1.05	4.0	469
T3	248	1.81	1.05	3.9	523, ~407 (sh)
T4	1762	1.86	1.04	4.1	399, 422, 450, 485, 521,569, 620, ~378 (sh), ~696 (sh)
T5	4530	1.83	1.02	4.7	407, 416, 426, 437, 449, 461, 475, 489, 504, 520, 537, 555, 576, 597, 620, 645, 672, 702,389 (sh), 398 (sh), 738 (sh)

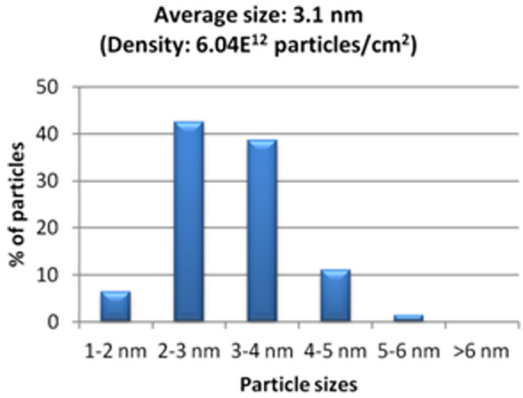

FIG. 4. Average size, density, and size distribution of particles for samples T1 and T5. More than 81% of the particles found have sizes between 2 and 4 nm.

only the one obtained for sample T5 is reported. The calculation of the mean size value and variance from the histogram was done using the equations: $\mu = \sum x \cdot p(x)$ and $\sigma^2 = \sum x^2 \cdot p(x) - \mu^2$, respectively, where p(x) is the probability of occurrence and x is the size mean value in the corresponding range. A mean size value of $\mu = 3.085$ nm and a variance of $\sigma^2 = 0.6747$ nm was obtained. A Kolmogorov-Smirnov normality test was performed as well and it was found that the behavior can be very well approximated to a normal distribution with a standard deviation of $\sigma = 0.8214$ nm from the mean value. Finally, to calculate the particle density, the number of particles and the area in nm^2 were obtained for each micrograph using the image acquisition software included with the HRTEM microscope. The result was 0.0604 particles/nm^2, which is equivalent to 6.04×10^{12} particles/cm^2.

B. Photoluminescence and optical transmittance

Fig. 5 shows the PL spectra of samples T1 (31 nm), T2 (95 nm), and T3 (248 nm). As expected, the intensity of the PL increases with thickness. It is also observed from this figure that the features of the PL spectra of the samples T1 and T2, whose thickness are lower than 100 nm, are similar, since they only show a single PL peak at ~469 nm. However, the spectrum of sample T3 has its main PL peak shifted up to 523 nm and presents a shoulder (sh) at ~407 nm. As Figure 6 shows, the PL spectrum of sample T4 (1764 nm) is much more intense than the previous and presents seven peaks and two shoulders at wavelengths given in Table I. For the thickest sample, T5 (4530 nm), the PL signal is even more intense and presents eighteen peaks ant three shoulders (see Table I). In order to compare the average behavior of the PL spectra of the thickest samples with that of the thinnest, the PL spectra of the latter multiplied by a factor of 90 is also shown in Fig. 6. As it can be seen from the visual comparison of the spectra, the integrated PL signal of the thickest samples is very similar to that of the thinnest. This fact along with the increase of the number of PL peaks and the behavior of its positions with the sample thickness strongly suggests the existence of interference effects in the PL of the thick samples.

In order to show clearly the appearance of interference effects in the optical properties (emission, transmission and/or absorption of light) of the films, as their thickness increase above 100 nm, the PL spectra of samples T1, T3, T4, and T5, whose PL features change more significantly, and the corresponding optical transmission spectra of the same films deposited on quartz substrates, are plotted in Figures 7 and 8, respectively. As can be seen from these figures, the appearance of peaks and the increase in the number of peaks as the film thickness increases follows a similar trend in both, PL and transmittance spectra. As it is well known, oscillatory transmittance curves like those observed in samples T3, T4, and T5 of Fig. 7 are the result of interference of the transmitted light after multiple reflections within the film. The thickness (d) of the films can be estimated from these curves using the formula $d = \frac{\lambda_1 \lambda_2}{2n(\lambda_2 - \lambda_1)}$, where n is the average refractive index of the film in the spectral range, and λ_1 and λ_2 are the wavelengths of consecutive peaks. The thickness of samples T3, T4, and T5 estimated from this formula and using the refractive index given in Table I are shown in the corresponding spectra of Figure 8. Although this is a rough estimation of the thickness because the refractive index of the films is not constant in all the spectral range of the measurements, these thicknesses are of the same order of magnitude

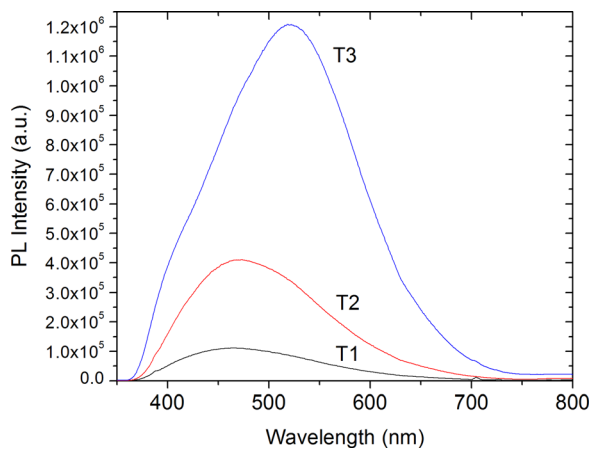

FIG. 5. PL spectra of samples T1, T2, and T3. The PL spectra of sample T3 is shifted towards ~523 nm and has a shoulder at ~403 nm.

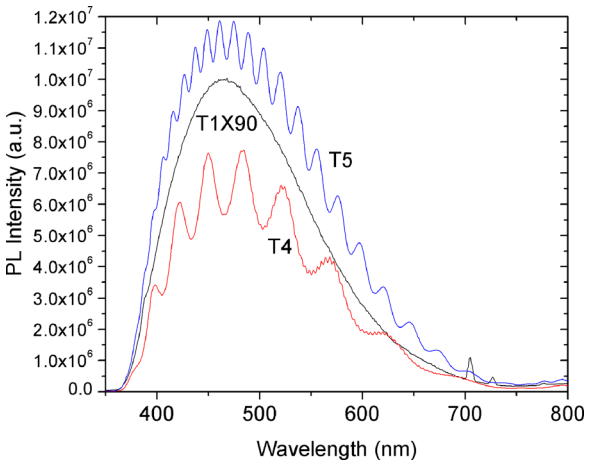

FIG. 6. PL spectra of samples T4 and T5, along with that of the PL spectrum of sample T1 multiplied by a factor of 90. The peaks appearing at wavelengths above 700 nm in the augmented PL spectra are due to spurious light during measurements.

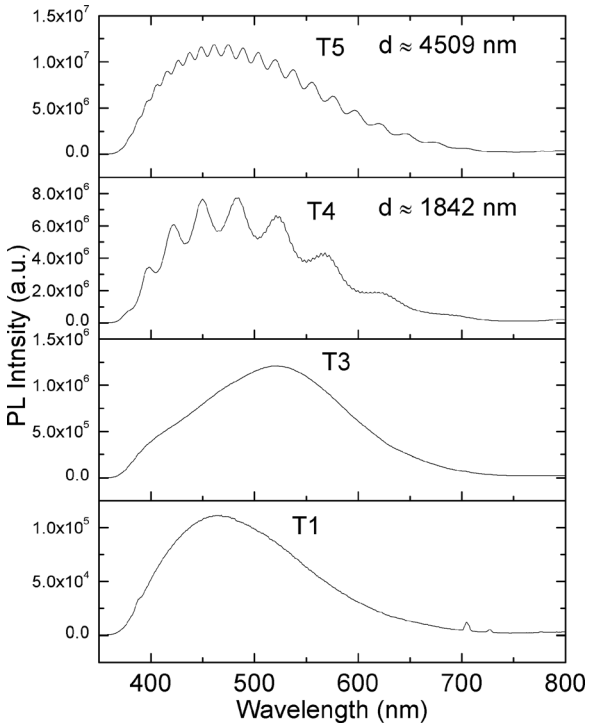

FIG. 7. PL spectra from films with different thickness, showing clearly the distortions generated in the PL spectra with respect to that of the thinnest sample, as the thickness increases above 200 nm.

compared with those measured by ellipsometry, given in Table I. The discrepancy between the values of thickness measured by ellipsometry and by interference in the transmittance can also be due to discrepancies in the deposition rate of the films, since they were deposited on different substrates (on silicon substrates for PL and ellipsometry measurements and on quartz substrates for transmittance measurements). Assuming that the oscillations in the PL spectra of films with thickness of few hundred nanometers or higher come from interference of multiple beam reflections in the films,[18,19,23] we also used the same formula $d = \frac{\lambda_1 \lambda_2}{2n(\lambda_2 - \lambda_1)}$ to calculate the thickness of the films from the PL spectra, and the values are shown in Fig. 7. The thickness estimations are also close to those measured by ellipsometry.

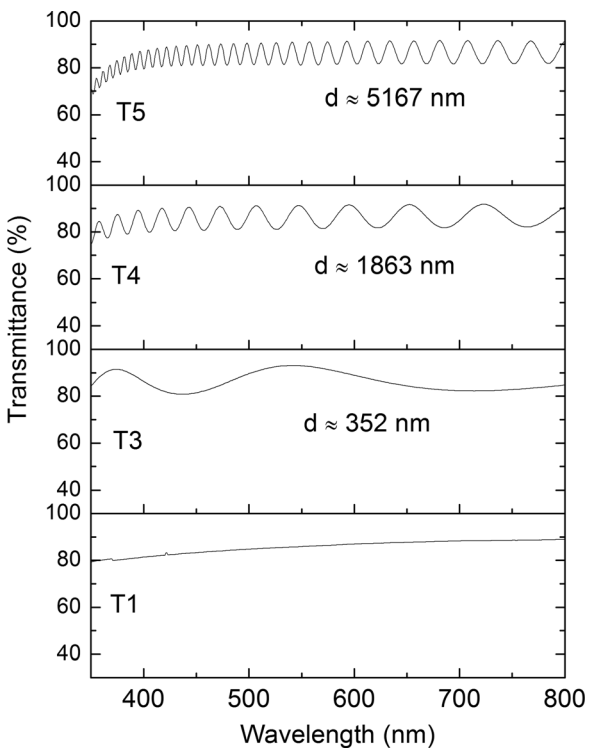

FIG. 8. Optical transmittance spectra for samples T1, T3, T4, T5 with different thickness deposited on quartz substrates.

IV. SIMULATION OF PL SPECTRA

A. Theoretical model

In this section, the basic physical phenomena behind interference effects on the luminescence spectra of a uniform film of luminescent particles (QDs) embedded in a homogeneous material is described. The mathematical details leading to our theoretical model, which is similar to that used to investigate the optical—geometrical effects on the PL spectra of Si nanocrystals embedded in SiO_2,[26] are summarized in the Appendix for future reference. Let us consider a composite film of thickness d and infinite lateral dimensions on a substrate. Let us suppose the incidence medium (medium 1) has a real refractive index n_1 whereas the substrate (medium 3) has a refractive index n_3, which may be complex. The luminescent QDs have dimensions much smaller than the wavelength of light, thus it is assumed that the film (medium 2) has a complex effective refractive index n_2 and conventional electrodynamics theory of continuous media is used. Consider the origin of our coordinate system at the interface between the film and the incidence medium as depicted in Fig. 9. As usual, the z-axis normal to the interfaces of the film is taken. Let us suppose the luminescent composite film is excited by a plane wave of vacuum wavelength λ_{exc}. The exciting wave will be absorbed within the film, but for thin films, this exciting wave may actually get multiply reflected at the interfaces resulting in a field whose amplitude oscillates inside the film. In any case, we can assume that a QD emits incoherently luminescent waves in all directions with amplitudes proportional to the amplitude of the exciting wave at the location of the QD as shown schematically in Figure 9. For a given λ_{exc}, the spectrum of the luminescent light will depend on the nature of the QDs and its surroundings as well as on temperature.

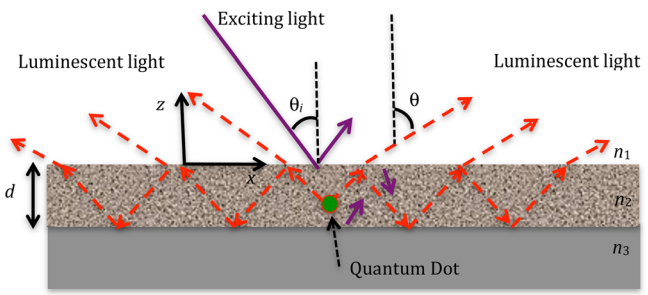

FIG. 9. Schematic of the composite film being excited at an oblique angle of incidence and emitting luminescent light back into the incidence medium. The multiple reflection process of a plane wave radiated upwards by a QD is also shown.

The intensity emitted out of a composite film of luminescent QD's embedded in a uniform matrix material can be modeled by regarding each radiating QD as a dipole antenna emitting incoherently with respect to all other nanoparticles. By incoherent, it is meant that light radiated by any two QDs has a random relative phase difference. The light waves radiated by any given QD and traveling up towards the interface with the incidence medium may be decomposed in a plane wave spectrum of *s* and *p* polarized waves. Correspondingly, light traveling down towards the interface with the substrate can also be decomposed in an *s* and *p* polarized plane wave spectrum. A plane wave component radiated downwards by a QD gets reflected specularly at the interface with the substrate and interferes with the plane wave component of the same polarization radiated upwards by the same QD and travelling in the same direction (in other words, the assumption is made that light fields radiated upwards or downwards by the same QD are coherent with respect to each other). Plane waves travelling in one direction within the film get multiply reflected between the interfaces and maintain a deterministic phase relationship among multiple reflections. Thus, all multiple reflections of one plane wave component interfere. At each reflection with the interfaces, a transmitted plane wave is generated. The coherent sum of all the transmitted waves to the incidence medium (air in the present case) results in the net luminescent output in a particular direction coming from a single QD. As already mentioned, light radiated by different QD is incoherent between each other. Thus, the total intensity of light radiated in one direction is the addition of the intensities coming from all QDs.

Assuming that QDs are uniformly distributed within a composite film of thickness d yields the following formula for the intensity emitted at frequency ω and at an angle θ:

$$I_\omega(\theta)=\rho D\cos^2\theta S^2(\omega)\int_0^d U(d,n_1,n_2,n_3,z)|\exp[ik_{z2}z]|^2 I_{exc}(z)dz, \tag{1}$$

where

$$U(d,n_1,n_2,n_3,z)=\frac{1}{2}\left|\frac{1+r_{23}^s\exp[2ik_{z2}(d-z)]}{1-r_{21}^s r_{23}^s\exp[2ik_{z2}d]}\right|^2|t_{21}^s|^2 + \frac{1}{2}\left|\frac{1-r_{23}^p\exp[2ik_{z2}(d-z)]}{1-r_{21}^p r_{23}^p\exp[2ik_{z2}d]}\right|^2|t_{21}^p|^2, \tag{2}$$

ρ is the number density of QDs, D is an experimental constant, θ is the viewing angle, $S(\omega)$ is the normalized luminescence spectra of an isolated QD embedded in the matrix excited at λ_{exc}, $k_{z2}=k_0\sqrt{n_2^2-n_1^2\sin^2\theta}$ where n_2 is the effective refractive index of the composite film, n_1 is the refractive index of the incidence medium (air), r_{ab}^c and t_{ab}^c are the Fresnel reflection and transmission coefficients for c (either *s* or *p*) polarized plane waves for light incident from medium a (1, 2 or 3) to the interface with medium b (1, 2, or 3) with the appropriate wave-vector (see the Appendix for details), and $I_{exc}(z)$ is the intensity of the excitation light field inside the composite film. The integral in Eq. (1) is readily done numerically.

All experimental data in this work were obtained at a normal viewing angle ($\theta=0$). In this case, $k_{z2}=k_0 n_2$, $r_{ab}^s=-r_{ab}^p$, and $t_{ab}^s=t_{ab}^p$, thus the two terms on the right hand side of Eq. (2) become equal and the function U simplifies accordingly.

V. COMPARISON OF SIMULATED WITH EXPERIMENTAL SPECTRA

To compare the model with the experimental spectra, the dispersion of the refractive index of the PL composite medium was first estimated so that the PL spectrum obtained from Eq. (1) would reproduce better the PL spectra of all samples assuming the nominal thicknesses for each sample (see Table I). We estimated

$$n_2=1.825+0.002\left(\frac{450}{\lambda}\right)^4+0.005\left(\frac{650}{\lambda}\right)^2+i0.005. \tag{3}$$

For the sake of simplicity, the dispersion of the substrate's refractive index was ignored within the range of wavelengths of the emission spectrum and its value was considered constant and given by $n_3=3.85+i0.03$. However, at the excitation wavelength, we took into account normal dispersion of the substrate refractive index and used $n_2^{exc}=3.95+i0.04$. For the luminescent film, it was assumed $n_2^{exc}=1.95+i0.15$. We approximated the interference-free PL spectrum of the films (the function $S^2(\omega)$ defined above) as given by the PL spectrum of the thinnest sample (T1). The two spectra must be very close, since when the thickness of the film tends to zero, the interference effects must vanish. The PL spectra of the remaining samples were subsequently simulated by adjusting slightly the thickness of the films.

The normalized experimental and simulated PL spectra for samples T3, T4, and T5 are presented in Figures 10–12. As shown in Figure 10, the incorporation of interference effects in the simulated spectrum reproduces qualitatively well the shift of the main peak toward higher wavelengths and the shoulder that is observed in the corresponding

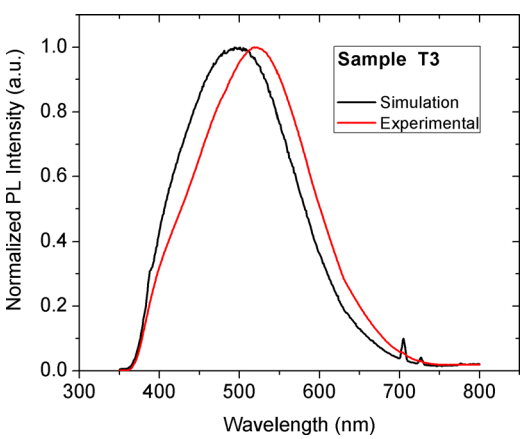

FIG. 10. Normalized simulated and experimental PL spectra for sample T3. The thickness d used to simulate this PL spectrum was 240 nm.

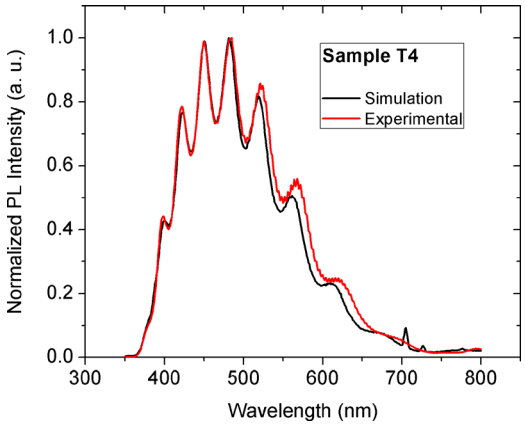

FIG. 11. Normalized simulated and experimental PL spectra for sample T4. The thickness d used in the simulated PL spectrum was 1775 nm.

experimental spectrum, compared with that of the thinnest sample T1 where there are no interference effects (undistorted spectrum). On the other hand, as can be seen from Figures 11 and 12, corresponding to the thicker samples T4 and T5, our interference formulas (1) and (2) predict very accurately the number of maxima and minima in the simulated PL spectra and their positions, as a function of thickness, compared with that of the experimental PL spectra. Additionally, the thickness d used in formulas (1) and (2), for reproducing the simulated PL spectra of Figures 10 to 12 were 240 nm, 1775 nm, and 4340 nm, respectively, which are very close to those measured by ellipsometry, T3 (248 nm), T4 (1762 nm), and T5 (4530 nm). The relatively small discrepancies between the simulated and experimental spectra can be originated by small changes in the intrinsic emission spectrum (undistorted spectrum) and intrinsic optical properties of the films as a function of thickness, probably due to mechanical stress effects. In order to support this, it is worth mentioning that, for instance, the imaginary part of the refractive index n_2 used for the simulation of sample T5 was increased to 0.011 for better fitting of the simulation of the depth of the interference spectral-fringes. Further adjustments of the refractive index of media 2 and 3 and the excitation wavelength could reduce the differences between the experimental and simulated spectra. However, these

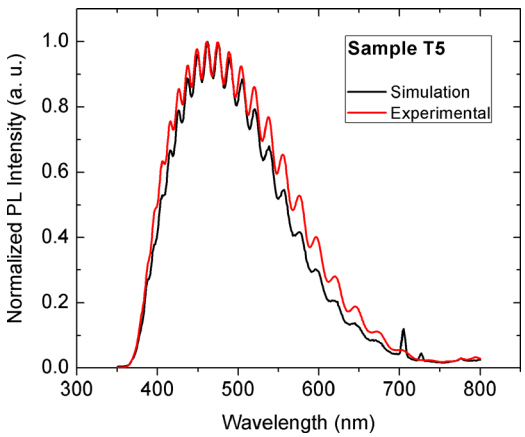

FIG. 12. Normalized simulated and experimental spectra for sample T5. In this case, the thickness d used for the simulation of the PL spectrum was 4340 nm.

adjustments would differ noticeably from sample to sample and are out of the scope of this work. Our intention here is simply to corroborate that the multiple peaks appearing in the PL spectra of the thickest two samples are due to interference effects.

VI. CONCLUSIONS

The effect of film thickness on the PL of Si-QDs embedded in SiN_x films with approximately the same composition and nanostructure have been investigated experimentally and theoretically. The experiments show that the increase of the thickness of these films above a few hundreds of nanometers produces significant distortions on the PL spectra of films, such as peak shifts and the appearance of shoulders together with multiple peaks. Theoretical simulations have demonstrated that these distortions are mainly due to interference effects and not to intrinsic changes in the films. The model used to simulate the PL spectra as a function of film thickness is versatile enough to improve the fitting with the experimental spectra by changing some optical parameters and can be helpful to further investigate the intrinsic optical properties of the films.

ACKNOWLEDGMENTS

The technical assistance of L. Huerta, R. Hernández-Reyes, M. A. Canseco, J. M. García-León, and J. Camacho is greatly acknowledged. This research work was partially supported under Project PAPIIT-UNAM Nos. IN115711 and IN106712.

APPENDIX: RIGOROUS DERIVATION OF THE THEORETHICAL MODEL

Consider a thin film with a uniform distribution of very small QDs as depicted in Fig. 9. The coordinate system is placed with its origin at the upper surface of the thin film with the z-axis normal to the thin film's surface and pointing inwards as indicated in Figure 9. The exciting light is linearly polarized and its electric field is given by $\mathbf{E}^{exc} = E_0 \exp(i\mathbf{k}_1^{exc} \cdot \mathbf{r} - i\omega t)\hat{\mathbf{e}}$,where $\hat{\mathbf{e}}$ is a unit vector perpendicular to the incident wave vector k^i. The exciting wave enters the thin film and part of its energy is absorbed by the particles, which in turn emit light with a broadband spectrum in all directions. Light emitted by any of the particles is multiply reflected by the interfaces of the thin film containing the particles. Suppose the incident wave vector is in the xz plane. Consequently, $\mathbf{k}_1^{exc} = k_{x1}^{exc}\hat{\mathbf{a}}_x - k_{z1}^{exc}\hat{\mathbf{a}}_z$ where $k_{x1}^{exc} = k_0 n_1 \sin\theta_i$ and $k_{z1}^{exc} = k_0 n_1 \cos\theta_i$, where θ is the angle of incidence. In general, the electric field at the exciting wavelength within the thin film is given by

$$\mathbf{E}_{ThF}^{exc} = a\exp(ik_{x1}^{exc}x - ik_{z2}^{exc}z - i\omega_{exc}t)\hat{\mathbf{e}}_{2-} + b\exp(ik_{x1}^{exc}x + ik_{z2}^{exc}z - i\omega_{exc}t)\hat{\mathbf{e}}_{2+}, \quad \text{(A1)}$$

where $k_{z2}^{exc} = k_0(n_2^2 - n_1^2\sin^2\theta_i)^{1/2}$and n_2 is the complex refractive index of the thin film at the exciting wavelength, $\hat{\mathbf{e}}_{2-}$ and $\hat{\mathbf{e}}_{2+}$ are the corresponding polarization vectors, and

$$a = \frac{(1+r')}{(1+r'_{23}\exp[2ik_{z2}^{exc}d])}, \quad b = ar'_{23}\exp[2ik_{z2}^{exc}d],$$
$$r' = \frac{r_{12}' + r_{23}'\exp(2ik_{z2}^{exc}d)}{1 + r_{12}' r_{23}'\exp(2ik_{z2}^{exc}d)}, \tag{A2}$$

where r'_{ab} is the reflection coefficient for linearly polarized plane waves for light incident from medium a to the interface with medium b. The primes on the reflection coefficients indicate they are to be evaluated at the exciting wavelength. The reflection coefficients are for either s or p polarization accordingly to the polarization of the incident wave.

To construct the luminescent spectra of a single QD embedded inside a thin film, first consider a luminescent particle, say the nth particle, within a boundless medium of refractive index n_2. It absorbs energy from the incident wave and radiates light at other wavelengths. The electric field radiated by the nth particle at frequency ω may be expressed in terms of the electric-field Green's function dyadic $\vec{\mathbf{G}}$ for monochromatic waves in the medium surrounding the particles and an excess current $\mathbf{J}_n^{ind}$ induced at frequency ω within the particle as[28]

$$\mathbf{E}_n^{lum}(\mathbf{r};\omega) = i\omega\mu_0 \int_V d^3r' \vec{\mathbf{G}}(\mathbf{r},\mathbf{r}';\omega)\cdot\mathbf{j}_n^{ind}(\mathbf{r}';\omega), \tag{A3}$$

with

$$\mathbf{J}_n^{lum}(\mathbf{r};\omega) = \mathbf{j}(\omega)\delta(\mathbf{r}'-\mathbf{r}_n)S(\omega)|\mathbf{E}_{ThF}^{exc}(\mathbf{r}_n)|, \tag{A4}$$

where $\mathbf{r}_n$ is the position of the particle, $S(\omega)$ is the normalized spectral emission function of the QDs when excited with light of frequency λ_{exc}, with dimensions of current and inverse of an electric field. We assume that the induced currents radiating the luminescent waves are proportional to the exciting field at the position of the luminescent particle $|\mathbf{E}_{ThF}^{exc}(\mathbf{r}_n)|$. The vector function $\mathbf{j}(\omega)$ in Eq. (A4) has unit magnitude, it is dimensionless and takes into account the polarization of the re-emitted light. The Dyadic Green's function can be expanded in a plane wave spectrum in the half-spaces above and below the particle.[28] Thus, the Green's function is expressed by

$$\vec{\mathbf{G}}(\mathbf{r},\mathbf{r}\prime) = \frac{i}{8\pi^2}\int dk_x dk_y \frac{(\vec{\mathbf{I}} - \hat{\mathbf{k}}_\pm\hat{\mathbf{k}}_\pm)}{k_z}\exp[i\mathbf{k}_\pm\cdot(\mathbf{r}-\mathbf{r}')], \tag{A5}$$

where $\mathbf{k}_\pm = k_x\hat{\mathbf{a}}_x + k_y\hat{\mathbf{a}}_y \pm k_z\hat{\mathbf{a}}_z$ and $k_z = (k_0^2 n_2^2 - k_x^2 - k_y^2)^{1/2}$. The plus and minus signs are used for $z > z'$ and $z < z'$, respectively. Introducing Eq. (A5) in Eq. (A3) and performing the integral over d^3r' yields

$$\mathbf{E}_n^{lum}(\mathbf{r};\omega) = \frac{-\omega\mu_0}{8\pi^2}\int dk_x dk_y \frac{(\vec{\mathbf{I}} - \hat{\mathbf{k}}_+\hat{\mathbf{k}}_+)}{k_z} \cdot \mathbf{j}(\omega)\exp[i\mathbf{k}_+\cdot(\mathbf{r}-\mathbf{r}_n)]S(\omega)|\mathbf{E}_{ThF}^{exc}(\mathbf{r}_n)|, \tag{A6}$$

for $z > z_n$ and

$$\mathbf{E}_n^{lum}(\mathbf{r};\omega) = \frac{-\omega\mu_0}{8\pi^2}\int dk_x dk_y \frac{(\vec{\mathbf{I}} - \hat{\mathbf{k}}_-\hat{\mathbf{k}}_-)}{k_z} \cdot \mathbf{j}(\omega)\exp[i\mathbf{k}_-\cdot(\mathbf{r}-\mathbf{r}_n)]S(\omega)|\mathbf{E}_{ThF}^{exc}(\mathbf{r}_n)|, \tag{A7}$$

for $z < z_n$. These are the fields radiated above and below the nth QD expressed in terms of their plane wave spectra.

Finally, the interfaces at $z = 0$ and $z = -d$ are incorporated into the model. A plane wave inside the *Kernel* in Eq. (A6) with wave vector $\mathbf{k}_+$ and polarization $(\vec{\mathbf{I}} - \hat{\mathbf{k}}_+\hat{\mathbf{k}}_+)\cdot\mathbf{j}(\omega)$ gets multiply reflected between both interfaces. At each reflection on the upper interfaces, it is partially transmitted to the upper medium ($z < 0$). The wave initially emitted with $\mathbf{k}_-$ in Eq. (A7) also gets multiply reflected between the interfaces and every time it reflects on the upper interface it transmits partially to the upper medium. All plane waves transmitted to the upper medium in a particular direction coming from the radiation of the particle at $\mathbf{r}_n$ add up coherently.

Note that every time a wave with wave-vector $\mathbf{k}_+$ and polarization $(\vec{\mathbf{I}} - \hat{\mathbf{k}}_+\hat{\mathbf{k}}_+)\cdot\mathbf{j}(\omega)$ gets reflected in the upper interface a wave with wave-vector $\mathbf{k}_-$ and polarization $\pm(\vec{\mathbf{I}} - \hat{\mathbf{k}}_-\hat{\mathbf{k}}_-)\cdot\mathbf{j}(\omega)$ is generated, where the + or − sign is for s or p polarization, respectively; and every time, a wave with wave-vector $\mathbf{k}_-$ and polarization $(\vec{\mathbf{I}} - \hat{\mathbf{k}}_-\hat{\mathbf{k}}_-)\cdot\mathbf{j}(\omega)$ is reflected at the lower interface, a wave with wave-vector $\mathbf{k}_+$ and polarization $\pm(\vec{\mathbf{I}} - \hat{\mathbf{k}}_+\hat{\mathbf{k}}_+)\cdot\mathbf{j}(\omega)$ is generated. The corresponding reflection coefficients are the standard Fresnel reflection coefficients found in many text books, r_{21} at upper interface ($z = 0$) and r_{23} at the lower interface ($z = -d$), for either s or p polarized waves.

Adding up the initial wave radiated upwards with wave vector $\mathbf{k}_+$ and all of its multiple reflections gives

$$(\vec{\mathbf{I}} - \hat{\mathbf{k}}_+\hat{\mathbf{k}}_+)\cdot\mathbf{j}(\omega)\{\exp[-ik_{z2}z_n] + r_{21}r_{23}\exp[-ik_{z2}z_n] \times \exp[2ik_{z2}d] + (r_{21}r_{23})^2\exp[-ik_{z2}z_n]\exp[4ik_{z2}d] + ...\} \times \exp[i\mathbf{k}_+\cdot\mathbf{r}].$$

Adding up the initial wave radiated downwards with wave vector $\mathbf{k}_-$ and reflected with a wave vector $\mathbf{k}_+$ with all subsequent multiple reflections gives

$$\pm\exp[i\mathbf{k}_+\cdot\mathbf{r}]\{r_{23}\exp[ik_{z2}(z_n+d)]\exp[ik_{z2}d] + r_{23}^2 r_{21} \times \exp[ik_{z2}(z_n+d)]\exp[3ik_{z2}d] + r_{23}^3 r_{21}^2\exp[ik_{z2}(z_n+d)] \times \exp[5ik_{z2}d] + ...\}(\vec{\mathbf{I}} - \hat{\mathbf{k}}_+\hat{\mathbf{k}}_+)\cdot\mathbf{j}(\omega),$$

where as already said the + sign is for s polarization and the − sign is for p polarization. Adding together the latter two series and simplifying gives

$$(\vec{\mathbf{I}} - \hat{\mathbf{k}}_+\hat{\mathbf{k}}_+)\cdot\mathbf{j}(\omega)\left(\frac{\exp[-ik_{z2}z_n]}{1 - r_{21}^c r_{23}^c\exp[2ik_{z2}d]} \pm \frac{r_{23}^c\exp[-ik_{z2}(d+z_n)]\exp(ik_{z2}d)}{1 - r_{23}^c r_{21}^c\exp[2ik_{z2}d]}\right)\exp[i\mathbf{k}_+\cdot\mathbf{r}], \tag{A8}$$

where the subscript c was added to the reflection coefficients to indicate the polarization. It can be either s or p for the corresponding polarization. The standard Fresnel reflection coefficients for non-magnetic media ($\mu_1 = \mu_2 = \mu_3 = \mu_0$) can be written as

$$r_{ab}^{s} = \frac{k_{za} - k_{zb}}{k_{za} + k_{zb}} \quad \text{and} \quad r_{ab}^{p} = \frac{\varepsilon_b k_{za} - \varepsilon_a k_{zb}}{\varepsilon_b k_{za} + \varepsilon_a k_{zb}}, \tag{A9}$$

where a and b are either 1, 2, or 3, ε_1, ε_2, and ε_3 are the electric permittivity of media 1, 2, and 3, respectively, and

$$k_{zq} = (k_0^2 n_q^2 - k_x^2 - k_y^2)^{1/2}, \tag{A10}$$

where q is either 1, 2, or 3.

The total field traveling in the direction of $\mathbf{k}_+$ gets transmitted to the upper medium with a wave vector $\mathbf{k}_1 = k_x \hat{\mathbf{a}}_x + k_y \hat{\mathbf{a}}_y + k_{z1} \hat{\mathbf{a}}_z$ with $k_{z1} = k_0 \cos\theta$. The amplitude of the transmitted wave acquires the factor, either

$$t_{21}^{s} = \frac{2k_{z2}}{k_{z2} + k_{z1}} \quad \text{or} \quad t_{21}^{p} = \sqrt{\frac{\varepsilon_2}{\varepsilon_1}} \frac{2\varepsilon_1 k_{z2}}{\varepsilon_1 k_{z2} + \varepsilon_2 k_{z1}}. \tag{A11}$$

These are the standard Fresnel transmission coefficients at the interface between medium 2 and medium 1.

The total luminescent field emitted to the upper hemisphere from the luminescent particle at $\mathbf{r}_n$ is given by

$$\mathbf{E}_n^{lum}(\mathbf{r};\omega) = \frac{-\omega\mu_0}{8\pi^2} \int dk_x dk_y \frac{(\vec{\mathbf{I}} - \mathbf{k}_1\mathbf{k}_1)}{k_z} \cdot \mathbf{j}(\omega) \times \left\{ \left(\frac{\exp[-ik_{z2}z_n] \pm r_{23}\exp[2ik_{z2}d]\exp(ik_{z2}z_n)}{1 - r_{21}r_{23}\exp[2ik_{z2}d]} \right) \times t_{21}\exp[i\mathbf{k}_1 \cdot \mathbf{r}] \right\} S(\omega) |\mathbf{E}_{ThF}^{exc}(\mathbf{r}_n)| \tag{A12}$$

simplifying the expression within parentheses. If the observation point is in the far zone (that is r is very large), the integral can be evaluated using the method of stationary phase.[29] Once having the far field the luminescent intensity is found to be $I_n^{lum} = \frac{1}{2}(k_1/\omega\mu_0)|\mathbf{E}_n^{lum}|^2$. Assuming that the polarization of the emitted light is random the average between the results for s polarization and p polarizations is taken

$$I_n^{lum}(r,\theta,\phi;\omega;z_n) = \frac{1}{2}(k_1/\omega\mu_0)\left(\frac{\omega\mu_0 k_1}{4\pi r}\right)^2 \times \cos^2\theta Q(d,n_1,n_2,n_3,\omega,z_n) S^2(\omega) I_{exc}(z_n) \tag{A13}$$

with $I_{exc}(z_n) = |\mathbf{E}_{ThF}^{exc}(\mathbf{r}_n)|^2$ and

$$Q(d,n_1,n_2,n_3,\omega,z_n) = \frac{1}{2}\left|\frac{\exp[-ik_{z2}z_n] + r_{23}^{s}\exp[2ik_{z2}d]\exp(ik_{z2}z_n)}{1 - r_{21}^{s}r_{23}^{s}\exp[2ik_{z2}d]}\right|^2 |t_{21}^{s}| + \frac{1}{2}\left|\frac{\exp[-ik_{z2}z_n] - r_{23}^{p}\exp[2ik_{z2}d]\exp(ik_{z2}z_n)}{1 - r_{21}^{p}r_{23}^{p}\exp[2ik_{z2}d]}\right|^2 |t_{21}^{p}|, \tag{A14}$$

where k_x and k_y inside the expressions for r_{21}^{c}, r_{23}^{c}, and t_{21}^{c} [see Eqs. (A9) and (A11)] for either polarization ($c = $ s or p) are evaluated at the stationary point obtained upon evaluating the integrals in Eq. (A11) by the method of stationary phase, $k_x = k_0 n_1 \sin\theta\cos\phi$ and $k_y = k_0 n_1 \sin\theta\sin\phi$, where θ and ϕ are the angles of the viewing direction (in spherical coordinates). Note that k_{zq} in Eq. (A10)

$$k_{zq} = k_0(n_q^2 - n_1^2\sin^2\theta)^{1/2}. \tag{A15}$$

The total luminescence intensity along a given direction of observation (in the far zone) is obtained by multiplying the latter equation times the number density of luminescent particles, ρ, and integrating on $dx_n dy_n dz_n$ over the volume of the film illuminated by the exciting field. The illuminated area is assumed to be large but finite and it is denoted as A. Since in the far field, the intensity does not depend on the lateral position of the particles the integrals over $dx_n dy_n$ gives the factor A and we get

$$I(r,\theta,\phi;\omega) = \rho A \int_{-d}^{0} dz_n I_n^{lum}(r,\theta,\phi;\omega;z_n). \tag{A16}$$

Using Eqs. (A13) and (A14) in Eq. (A16), making the change of variable $z = -z_n$ and defining the experimental constant D, as $A\frac{1}{2}(k_1/\omega\mu_0)(\omega\mu_0 k_1/4\pi r)^2$ yields Eq. (1) in the text.

[1] L. Pavesi, L. Dal Negro, C. Mazzoleni, G. Franzò, and F. Priolo, Nature **408**, 440 (2000).
[2] L. Dal Negro, J. H. Yi, J. Michel, L. C. Kimerling, S. Hamel, A. Williamson, and G. Galli, IEEE J. Sel. Top. Quantum Electron. **12**, 1628 (2006).
[3] J. C. Alonso, F. A. Pulgarín, B. M. Monroy, A. Benami, M. Bizarro, and A. Ortiz, Thin Solid Films **518**, 3891 (2010).
[4] R. Huang, J. Song, X. Wang, Y. Q. Guo, C. Song, Z. H. Zheng, X. L. Wu, and P. K. Chu, Opt. Lett. **37**, 692 (2012).
[5] J. De la Torre, G. Bremond, M. Lemiti, G. Guillot, P. Mur, and N. Buffet, Thin Solid Films **511–512**, 163 (2006).
[6] E. Cho, M. A. Green, G. Conibeer, D. Song, Y. H. Cho, G. Scardera, S. Huang, S. Park, X. J. Hao, Y. Huang, and L. Van Dao, Adv. OptoElectron. **2007**, 1.
[7] P. F. Trwoga, A. J. Kenyon, and C. W. Pitt, J. Appl. Phys. **83**, 3789 (1998).
[8] N. M. Park, C. J. Choi, T. Y. Seong, and S. J. Park, Phys. Rev. Lett. **86**, 1355 (2001).
[9] T. Y. Kim, N. M. Park, K. H. Kim, G. Y. Sung, Y. W. Ok, T. Y. Seong, and C. J. Choi, Appl. Phys. Lett. **85**, 5355 (2004).
[10] B. H. Kim, C. H. Cho, T. W. Kim, N. M. Park, G. Y. Sung, and S. J. Park, Appl. Phys. Lett. **86**, 091908 (2005).

[11]T. W. Kim, C. H. Cho, B. H. Kim, and S. J. Park, Appl. Phys. Lett. **88**, 123102 (2006).
[12]L. Dal Negro, J. H. Yi, L. C. Kimerling, S. Hamel, A. Williamson, and G. Galli, Appl. Phys. Lett. **88**, 183103 (2006).
[13]H. L. Hao, L. K. Wu, and W. Z. Shen, Appl. Phys. Lett. **92**, 121922 (2008).
[14]J. C. Alonso, G. Santana, A. Benami, and B. M. Monroy, in *Encyclopedia of Nanoscience and Nanotechnology* (2011), *pp.* 1–31.
[15]A. Rodriguez, J. Arenas, and J. C. Alonso, J. Lumin. **132**, 2385 (2012).
[16]H. Kato, N. Kashio, Y. Ohki, K. S. Seol, and T. Noma, J. Appl. Phys. **93**, 239 (2003).
[17]M. Molinari, H. Rinnert, and M. Vergnat, J. Appl. Phys. **101**, 123532 (2007).
[18]M. Anutgan, T. Anutgan, I. Atilgan, and B. Katircioglu, J. Lumin. **131**, 1305 (2011).
[19]Y. Liu, Y. Zhou, W. Shi, L. Zhao, B. Sun, and T. Ye, Mater. Lett. **58**, 2397 (2004).
[20]A. Zerga, M. Carrada, M. Amann, and A. Slaoui, Physica E **38**, 21 (2007).
[21]H. L. Hao, L. K. Wu, W. Z. Shen, and H. F. Dekkers, Appl. Phys. Lett. **91**, 201922 (2007).
[22]F. Delachat, M. Carrada, G. Ferblantier, J. J. Grob, and A. Slaoui, Nanotechnology **20**, 415608 (2009).
[23]A. Benami, G. Santana, A. Ortiz, A. Ponce, D. Romeu, J. Aguilar-Hernández, G. Contreras-Puente, and J. C. Alonso, Nanotechnology **18**, 155704 (2007).
[24]R. G. Elliman, M. J. Lederer, and B. Luther-Davies, Appl. Phys. Lett. **80**, 1325 (2002).
[25]S. M. Orbons, M. G. Spooner, and R. G. Elliman, J. Appl. Phys. **96**, 4650 (2004).
[26]R. Ferre, B. Garrido, P. Pellegrino, M. Perálvarez, C. García, J. a. Moreno, J. Carreras, and J. R. Morante, J. Appl. Phys. **98**, 084319 (2005).
[27]A. López-Suárez, J. Fandiño, B. M. Monroy, G. Santana, and J. C. Alonso, Physica E **40**, 3141 (2008).
[28]W. C. Chew, *Waves and Fields in Inhomogeneous Media* (IEEE Press, Piscataway, NJ, 1995), Chap. 7.
[29]R. E. Collin, *Antennas and Radiowave Propagation* (McGraw Hill, NY, 1985), Chap. 4.